Journal of Molecular Structure 1277 (2023) 134866

Contents lists available at ScienceDirect

Journal of Molecular Structure

journal homepage: www.elsevier.com/locate/molstr

Copper(II) chelates derived from an N,N,O-tridentate 2-pyridinecarboxaldehyde-N^4-phenylsemicarbazone: Synthesis, spectral aspects, crystal structure, FMO and NBO analysis

M. Sithambaresan[a,b], M. R. Prathapachandra Kurup[a,*], Goncagül Serdaroğlu[c], Savaş Kaya[d]

[a] Department of Applied Chemistry, Cochin University of Science and Technology, Kochi, Kerala 682 022, India
[b] Department of Chemistry, Faculty of Science, Eastern University, Chenkalady, Sri Lanka
[c] Sivas Cumhuriyet University, Math. and Sci. Edu., Sivas 58140, Turkey
[d] Sivas Cumhuriyet University, Health Services Vocational School, Department of Pharmacy, Sivas 58140, Turkey

ARTICLE INFO

Article history:
Received 8 September 2022
Revised 6 December 2022
Accepted 24 December 2022
Available online 25 December 2022

Keywords:
2-Pyridinecarboxaldehyde
Semicarbazone
Copper(II) chelate
EPR spectrum
Quantum chemical parameters
NBO analysis

ABSTRACT

Seven novel Cu(II) complexes [Cu(HPySc)Cl$_2$] (**1**), [Cu$_2$(PySc)$_2$(NO$_3$)$_2$]·H$_2$O (**2**), [Cu(HPySc)(SO$_4$)]·½H$_2$O (**3**), [Cu$_2$(PySc)$_2$(OAc)$_2$]·CH$_3$OH (**4**), [Cu$_2$(PySc)$_2$Br$_2$]·H$_2$O (**5**), [Cu(PySc)(NCS)]·2H$_2$O (**6**) and [Cu$_2$(PySc)$_2$(N$_3$)$_2$] (**7**) with 2-pyridinecarboxaldehyde-N^4-phenylsemicarbazone (HPySc) have been prepared and characterized using different analytical and spectroscopic techniques. The complex **6** is expected to be square planar while the other complexes are expected to be square pyramidal arrangement, among these, the geometry of complex **4** has been conformed by single crystal XRD study that it is a dimer and adopts distorted square pyramidal geometry around copper(II) centre. All the complexes are found to be paramagnetic and non-conductive in nature. The semicarbazone ligand is coordinated in neutral form in two of the complexes and in ionic form in others. DFT/B3LYP/6-311g**/LANL2DZ computations of the ligand HpySc (PyCHNNCONHPh) and seven Cu(II) complexes were performed to analyze the FMOs and important electron delocalizations that existed in each compound. Molecular stability and bond strengths have been investigated by applying natural bond orbital (NBO) analysis. All the complexes are more stable than the semicarbazone and the complex **2** is the most electronically stable (-5.160 eV) among the complexes. Furthermore, the semicarbazone is the hardest and complex **5** is the softest than all complexes due to the η values. The calculated energy gap between HOMO and LUMO energies show the variations of nucleophilic and electrophilic reactivity regions in the semicarbazone and in complexes **1-7**.

1. Introduction

The metal complexes of semicarbazones have received much attention from researchers and scientists because of their widespread biological and interesting structural properties [1–4]. They are the subject of considerable interest for the number of chemists due to the formation of transition metal complexes having different chemical, physical and structural properties [3]. The structure of the complex depends upon the type and the nature of the ligand and nature refers to the number of donor atoms, the flexibility between them and the ability to combine with metal ions. Interestingly, copper(II) complexes of pyridine based semicarbazones have interesting crystal structures involving diverse noncovalent interactions [5].

Semicarbazones are also found to have anti-Trypanosoma cruzi activity [6]. Moreover, the biological activities of their complexes could be due to metal ion coordination. Semicarbazones are also used as inhibitors in different biological processes. 2-Hydroxy-1-naphthaldehyde semicarbazone was employed as a new Jack bean urease inhibitor [7]. Semicarbazone derived from di-2-pyridyl ketone is found to have gelation properties [8].

Considering the above facts, we have prepared seven Cu(II) chelates with *2*-pyridinecarboxaldehyde-N^4-phenylsemicarbazone (HpySc, PyCHNNCONHPh) and different copper(II) salts. The magnetic parameters measured in EPR study are related to the structure of the paramagnetic complex, the number of ligands, nature of bonding and spatial arrangements of the ligands around the central metal ion. EPR spectroscopy is used as a powerful tool to deduce valuable information about the electronic environment of the paramagnetic Cu(II) center [9]. Electronic spectroscopy, IR spectroscopy and thermogravimetric analysis have been carried out to confirm the coordination of ligands and the presence of water molecules in

* Corresponding author.
E-mail addresses: mrp@cusat.ac.in, mrp@cukerala.ac.in (M. R.P. Kurup).

https://doi.org/10.1016/j.molstruc.2022.134866
0022-2860/

the complexes. Natural Bond Orbital (NBO) analysis was also done to understand the main intramolecular interactions which stabilize the chelates [10].

2. Experimental

2.1. Materials

Copper acetate monohydrate, copper chloride, copper sulphate pentahydrate, sodium azide, potassium thiocyanate, copper bromide, copper nitrate (all are BDH, AR grade) were used without further purification. All solvents were purified by standard methods.

2.2. Synthesis of the semicarbazone and its Cu(II) chelates

2-Pyridinecarboxaldehyde-N^4-phenylsemicarbazone (HPySc, PyCHNNCONHPh) is prepared by adapting a method reported by us [11]. Yield: 72%; m.p.: 168-171 °C; Elemental Anal. Found (Calcd.) (%): C,72.47 (72.13); H, 5.20 (5.10); N, 18.14 (17.71). UV spectral data (nm): n→π^*=312, $\pi\rightarrow\pi^*$=262 and 235; FT IR data (cm^{-1}): ν(C=N)=1597, ν(N–N)=1143, $\nu(^4$N–H)=3107, $\nu(^2$N–H)=3372, (C=O)=1693; ^{1}H NMR spectral data (ppm): δ 9.75 (s, 1H, ^{2}N), δ 8.39 (s, 1H, 4N), δ 8.62 (d, 1H, ring C next to N) =7.0-8.0 (d & t. 7H, phenyl and pyridyl H).

[Cu(HPySc)Cl_2] (**1**)

A hot solution of the semicarbazone, HPySc (0.240 g, 1 mmol) in methanol (20 mL) was mixed with $CuCl_2{\cdot}2H_2O$ (0.170 g, 1 mmol) in methanol (10 mL) with constant stirring. The mixture was then stirred for 4 hours. The complex formed was filtered, washed thoroughly with water, methanol and ether and finally dried over P_4O_{10} *in vacuo*.

Yield: 85.4%; Elemental Anal. Found (Calcd.) (%): C, 41.51 (41.67); H, 3.66 (3.23); N, 15.27 (14.95). Molar conductivity (Λ_m) =24 $ohm^{-1}cm^2mol^{-1}$ in 10^{-3} M DMF at 298 K, μ (B.M.) = 1.826. Thermal data: weight loss of 57% at 220 °C; weight loss of 19% at 250–600 °C.

[Cu_2(PySc)$_2$(NO_3)$_2$]·H_2O (**2**)

A hot methanolic solution (15 mL) of HPySc (0.240 g, 1 mmol) was added to a methanol solution (10 mL) of $Cu(NO_3)_2{\cdot}3H_2O$ (0.241 g, 1 mmol). The mixture was stirred for 3 hours. The formed product was filtered, washed with water, ethanol and ether and dried *in vacuo* over P_4O_{10}.

Yield: 39.1%; Elemental Anal. Found (Calcd.) (%): C, 41.33 (40.79); H, 3.25 (3.42); N, 18.82 (18.29), Molar conductivity (Λ_m) =52 $ohm^{-1}cm^2mol^{-1}$ in 10^{-3} M DMF at 298 K, μ (B.M.) = 1.037. Thermal data: weight loss of 2.4% at 130–150 °C; weight loss of 78% at 250 °C.

[Cu(HPySc)(SO_4)]·½H_2O (**3**)

The compound [Cu(HPySc)(SO_4)]·½H_2O (**3**) was obtained when a hot solution of HPySc (0.240 g, 1 mmol) in methanol (15 ml) was mixed with a hot filtered solution of $CuSO_4{\cdot}5H_2O$ (0.249 g, 1 mmol) in methanol (10 mL) with constant stirring. The mixture was then stirred for 5 hours and the resulting solution was kept for two days at room temperature. The crystals formed were separated, filtered, washed with ethanol, water and ether and then dried over P_4O_{10} *in vacuo*.

Yield: 75.2%; Elemental Anal. Found (Calcd.) (%): C, 38.10 (38.19); H, 3.29 (3.20); N, 13.82 (13.70); S, 7.45 (7.84), Molar conductivity (Λ_m) = 6 $ohm^{-1}cm^2mol^{-1}$ in 10^{-3} M DMF at 298 K, μ (B.M.) = 1.905. Thermal data: weight loss of 2.2% at 140–160 °C; weight loss of 55% at 220–500 °C.

[Cu_2(PySc)$_2$(OAc)$_2$]·CH_3OH (**4**)

A hot solution of HPySc (0.240 g, 1 mmol) in methanol (20 mL) was mixed with a hot filtered solution of $Cu(OAc)_2{\cdot}H_2O$ (0.199 g, 1 mmol) in water (10 mL) with constant stirring. The mixture was then stirred for 3 hours. Then the mixture was kept at room temperature for two days. On cooling, single crystals suitable for single-crystal XRD were collected.

Yield: 81.6%; Elemental Anal. Found (Calcd.) (%): C, 48.89 (49.26); H, 3.78 (4.26); N, 14.93 (14.82), Molar conductivity (Λ_m) =7.6 $ohm^{-1}cm^2mol^{-1}$ in 10^{-3} M DMF at 298 K, μ (B.M.) = 1.04. Thermal data: weight loss of 51.6% at 220–280 °C; weight loss of 14% at 280–400 °C.

[Cu_2(PySc)$_2Br_2$]·H_2O (**5**)

A hot solution of HPySc (0.240 g, 1 mmol) in methanol (10 ml) was mixed with a hot filtered solution of $CuBr_2$ (0.223 g, 1 mmol) in methanol (10 mL) with constant stirring. The mixture was stirred for 4 hours. The mixture was kept overnight at room temperature. The formed microcrystals were filtered, thoroughly washed with water, methanol and ether and finally dried over P_4O_{10} *in vacuo*.

Yield: 65.4%; Elemental Anal. Found (Calcd.) (%): C, 40.04 (39.86); H, 3.22 (3.09); N, 14.34 (14.30), Molar conductivity (Λ_m) =20 $ohm^{-1}cm^2mol^{-1}$ in 10^{-3} M DMF at 298 K, μ (B.M.) = 1.186. Thermal data: weight loss of 3.7% at 130–160 °C; weight loss of 59.2% at 200–430 °C.

[Cu(PySc)NCS]·$2H_2O$ (**6**)

A hot solution of HPySc (0.240 g, 1 mmol) in methanol (10 ml) was mixed with a hot filtered methanolic solution of potassium thiocyanate (0.097 g, 1 mmol). A hot filtered aqueous solution (10 mL) of $Cu(OAc)_2{\cdot}H_2O$ (0.199 g, 1 mmol, was added to this with constant stirring. The mixture was then refluxed for 3 hours. The complex separated as microcrystals was filtered and thoroughly washed with water, methanol and ether and finally dried over P_4O_{10} *in vacuo*.

Yield: 76.3%; Elemental Anal. Found (Calcd.) (%): C, 42.61 (42.36); H, 3.28 (3.81); N, 18.02 (17.64); S, 8.60 (8.08), Molar conductivity (Λ_m) =11 ohm^{-1} cm^2 mol^{-1} in 10^{-3} M DMF at 298 K, μ (B.M.) = 1.743. Thermal data: weight loss of 8.3 % at 130–160 °C; weight loss of 50% at 200–400 °C.

[Cu_2(PySc)$_2N_3$] (**7**)

A hot methanolic solution of HPySc (0.240 g, 1 mmol) (10 ml) was mixed with a hot filtered methanolic solution of sodium azide (0.065 g, 1 mmol). A hot filtered methanolic solution (10 mL) of $Cu(OAc)_2{\cdot}H_2O$ (0.199 g, 1 mmol) was added to this with constant stirring. The mixture was then refluxed for 3 hours. On cooling, microcrystals formed were filtered, thoroughly washed with water, methanol and ether and finally dried over P_4O_{10} *in vacuo*.

Yield: 87.6%; Elemental Anal. Found (Calcd.) (%): C, 45.10 (45.28); H, 2.49 (3.22); N, 28.20 (28.43), Molar conductivity (Λ_m) = 1 $ohm^{-1}cm^2mol^{-1}$ in 10^{-3} M DMF at 298 K, μ (B.M.) = 1.20. Thermal data: weight loss of 31% at 250–420 °C.

2.3. Physical measurements

Carbon, hydrogen and nitrogen content of semicarbazone and complexes were carried out using a Vario EL III CHNS analyzer

Table 1
Crystal refinement parameters of complex **4**.

Parameters	Compound, **4**
CCDC no	2131659
Empirical formula	$C_{31}H_{32}Cu_2N_8O_7$
Formula weight	755.75
Color	dark green
Temperature (T) K	293(2)
Wavelength (Mo Kα) (Å)	0.71073
Crystal system	monoclinic
Space group	$P2_1/c$
Cell parameters	
a	8.469(2) Å
b	10.759(4) Å
c	18.044(11) Å
α	90°
β	102.68(4)°
γ	90°
Volume V (Å^3)	1603.9(12)
Z	2
Calculated density (ρ) (Mg m^{-3})	1.565
Absorption coefficient, μ(mm^{-1})	1.387
F(000)	776
Crystal size mm^3	0.30 × 0.20 × 0.12
θ range for data collection	3.12 to 24.70°
Limiting indices	-9 ≤ h≤11, -12≤k≤14, -13≤l≤23
Reflections collected	6192
Unique Reflections (R_{int})	3652 [R(int) = 0.0692]
Completeness to θ	25.242 (61.9 %)
Absorption correction	Semi-empirical from equivalents
Maximum and minimum transmission	0.824 and 0.704
Refinement method	Full-matrix least-squares on F^2
Data / restraints / parameters	1937/ 7 / 227
Goodness-of-fit on F^2	1.041
Final R indices [I > 2σ (I)]	R_1 = 0.0821, wR_2 = 0.2036
R indices (all data)	R_1 = 0.1228, wR_2 = 0.2262
Largest difference peak and hole (e Å^{-3})	0.897 and -0.698

$R_1 = \Sigma||F_o| - |F_c|| / \Sigma|F_o|$ $wR_2 = [\Sigma w(F_o^2-F_c^2)^2 / \Sigma w(F_o^2)^2]^{1/2}$.

at SAIF, Kochi, India. Infrared spectra were recorded on a Thermo Nicolet, AVATAR 370 DTGS model FT IR spectrophotometer as KBr pellets. Electronic spectra were recorded on a Cary 5000 version 1.09 UV-VIS- NIR spectrophotometer using solutions in DMF. The molar conductivities of the complexes in DMF solutions (10^{-3} M) at room temperature were measured using a Systronic model 303 direct reading conductivity meter. Magnetic measurements were made in the polycrystalline state on a vibrating sample magnetometer using Hg[Co(SCN)$_4$] as calibrant. The EPR spectra of polycrystalline samples at 298 K and solution at 77 K were recorded on a Varian E-112 X-band EPR spectrometer with 100- kHz field modulation. EPR spectra were simulated using EasySpin [12].

2.4. X-ray crystallography

Single crystals of compound $[Cu_2(PySc)_2(OAc)_2]\cdot CH_3OH$ (**4**) suitable for X-ray diffraction studies were grown from its methanolic solution by slow evaporation at room temperature. A single crystal of dimension 0.30 × 0.20 × 0.12 mm^3 was selected and mounted on an Oxford Diffraction Gemini X-ray diffractometer, equipped with Mo Kα (λ = 0.71073 Å) as the X-ray source. The crystallographic data along with details of structure solution refinements are given in Table 1. The unit cell dimensions were measured and the data collection was performed at 293(2) K. The structure was solved by direct methods and refined by full-matrix least-squares calculations with the SHELXL-2018/1 software [13]. The solvent methanol is disordered over two equivalent positions about a twofold rotation axis. The carbon oxygen distance of methanol molecule is restrained with DFIX instruction of 1.43 Å. The carbon and oxygen atoms of methanol molecule is made to have similar thermal ellipsoid parameters using SIMU instruction. Anisotropic refinement was performed for all non-hydrogen atoms and all H atoms on C atoms were placed in calculated positions with the aid of difference maps, with C–H bond distances of 0.93-0.97 Å and refined in the riding model approximation. The hydrogen atom attached to N4 was located from difference map and also refined with a riding model approximation. The molecular and crystal plots were made by DIAMOND version 3.2k [14]. The relevant bond lengths and bond angles are listed in Table 2.

Table 2
Selected bond lengths (Å) and bond angles (°) of $[Cu_2(PySc)_2(OAc)_2]\cdot CH_3OH$ (**4**).

Bond length		Bond angle	
Cu(1)–N(1)	1.937(7)	N(1)–Cu(1)-O(2)	100.7(3)
Cu(1)–O(2)	1.940(6)	N(1)–Cu(1)–O(1)	158<9(3)
Cu(1)–O(1)	2.008(7)	O(2)–Cu(1)–O(1)	100.3(3)
Cu(1)-N(2)	2.050(9)	N(1)–Cu(1)–N(2)	80.3(3)
Cu(1)–O(2)#1	2.401(6)	O(2)–Cu(1)–N(2)	170.8(3)
O(1)–C(1)	1.271(10)	O(1)–Cu(1)–N(2)	78.6(3)
Cu(1)···Cu(1) #1	3.398	N(1)–Cu(1)–O(2)#1	94.2(3)
		O(2)–Cu(1)–O(2)#1	111.7(3)
N(1)–C(8)	1.273(13)	O(1)–Cu(1)–O(2)#1	92.1(2)
N(2)–N(3)	1.341(11)	N(2)–Cu(1)–O(2)#1	111.7(3)
N(4)–C(7)	1.338(13)	C(7)–O(1)-Cu(1)	110.1(6)
N(3)–C(7)	1.351(12)	C(14)–O(2)–Cu(1)	119.2(6)
		C(14)–O(2)–Cu(1)#1	130.5(5)
N(4)–C(8)	1.376(14)	Cu(1)–O(2)–Cu(1)#1	102.5(3)
		C(6)–N(2)–N(3)	123.8(8)
		C(6)–N2)–Cu(1)	117.7(7)
		N(3)–N(2)-Cu(1)	118.3(7)

#1=-x,-y+1,-z+1.

2.5. Computational methods

All DFT/B3LYP [15,16] computations of ligand HPySc and seven Cu(II) complexes were performed by using LANL2DZ [17] for Cu atom and 6-311G** [18,19] for the remaining atoms. G09W [20] and GaussView 6.0.16 [21] packages were used to perform the quantum chemical computations and the analyzes and visualization of all computed results, respectively.

As known well, the ionization energy "*I*" and electron affinity "*A*" values for a neutral molecule can be approximated [22] by using HOMO and LUMO energies as defined below

$$I = -E_{HOMO}$$
$$A = -E_{LUMO}$$

In addition, the main QCPs "quantum chemical parameters" can be obtained from the "*I*" and "*A*" values

$$\chi = -\frac{I+A}{2}$$

$$\eta = \frac{I-A}{2}$$

$$\omega = \frac{\mu^2}{2\eta}$$

$$\Delta N_{max} = \frac{I+A}{2(I-A)}$$

Here, the abbreviations of QCPs are defined as χ → "electronic chemical potential" η → "global hardness", ω → "electrophilicity", and ΔN_{max} → "the maximum charge transfer capability index" [23–28].

Furthermore, ω- "the electron-donating power" and ω+ "the electron-accepting power" [29] can be calculated the following

equations

$$\omega^{+} \approx (I+3A)^2/(16(I-A))|$$
$$\omega^{-} \approx (3I+A)^2/(16(I-A))$$

The back-donation energy "$\Delta E_{back\text{-}donat.}$" [30] is successfully used to evaluate the chemical stability and hence reactivity of a relevant molecular system, especially having the Π- electronic and/or conjugated system.

$$\Delta\varepsilon_{back-donat.} = -\frac{\eta}{4}$$

Moreover, the electron delocalization and thus the reactivity tendency following the changing in the polarizability can be dealing with the NBOs "natural bond orbitals". For this reason, the second-order perturbation energy analysis results were used to appraise the dominant interactions that existed in each compound. In this method, the lowering of the stabilization energy for a specific donor (i) - acceptor (j) interaction, where ε_i and ε_j shows the energies of donor and acceptor orbitals, is defined [31–33] as follows

$$E^{(2)} = \Delta E_{ij} = qi\frac{(Fij)^2}{(\varepsilon j - \varepsilon i)}$$

In this equation, qi is "the donor orbital occupancy" and Fij is "the off-diagonal NBO Fock matrix element".

3. Results and discussion

3.1. Analytical measurements

Analytical data are in agreement with the assigned stoichiometries of the complexes. HPySc reacts with copper(II) salts in the molar ratio 1:1 to form monomeric complexes **1, 3**, and **6.** The ligand HPySc coordinates the metal in amido form in complexes **1** and **3** whereas it exists in monoanionic enolate form in complex **6**. The complexes **2, 4, 5**, and **7** are consistent with the general composition $Cu_2(PySc)_2Y_2$ where Y = NO_3, OAc, Br and N_3 respectively and the two copper atoms in **2, 5**, and **7** may be bridged through Y as in **4.**

The complexes are insoluble in most of the polar and non-polar solvents. Though some of the complexes are sparingly soluble in methanol all are soluble in DMF, and DMSO. The conductivity measurements were made in DMSO solutions and all complexes are found to be non-conductors [34].

The magnetic susceptibilities of the polynuclear complexes **2, 4, 5** and **7** suggest considerable interaction between metal centers and the magnetic moments fall in the range 1.037-1.20 B.M. and it can be assumed to be dinuclear in nature [35].

3.2. Crystal structure of complex 4

The single crystal X-ray diffraction study of the compound $[Cu_2(PySc)_2(OAc)_2]\cdot CH_3OH$ (**4**) reveals that this compound is a dimer bridged through the oxygen of the acetate moiety. The methanol molecule is present as a solvate in the complex. The molecular structure of the compound along with the atom numbering scheme is given in Fig. 1. The asymmetric unit is formed by one half of the molecule and the other half is related by a center of inversion in the Cu(1)–O(2)–Cu(1) #1–O(2)#1 (#1=-x,-y+1,-z+1) ring.

The lattice nature is monoclinic space group $P2_1/c$. This structure contains two copper centers where each center is pentacoordinate with azomethine nitrogen (N2), pyridyl nitrogen (N1), enolate oxygen (O1) of semicarbazone moiety and oxygens (O2, O2#1) from two acetate groups. The acetate group is monodentate as the other oxygen O3 is not coordinated to Cu(II). The compound exhibits a distorted square pyramidal geometry with the basal plane occupied by the semicarbazone ligand and the acetate oxygen (O2). Selected bond lengths (Å) and bond angles (°) of $[Cu_2(PySc)_2(OAc)_2]\cdot CH_3OH$ are presented in Table 2.

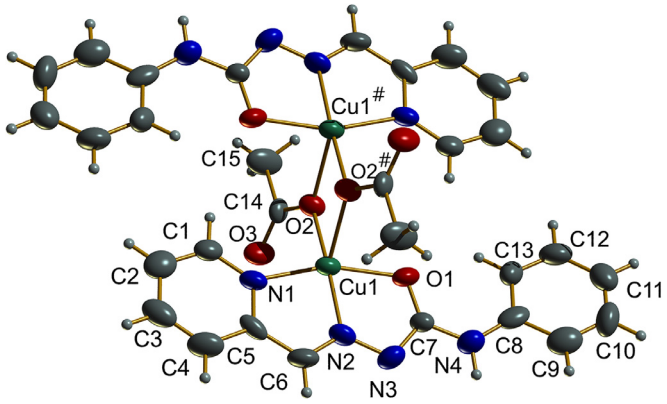

Fig. 1. The molecular structure of $[Cu_2(PySc)_2(OAc)_2]\cdot CH_3OH$ (**4**) along with the atom numbering scheme (solvent molecule is excluded for better clarity of the geometry; #: -x, 1-y,1-z).

The oxygen (O2)#1 (#1=-x,-y+1,-z+1) from the acetate group of the adjacent monomer plugs into the axial position resulting in a dimer with a Cu···Cu separation of 3.399 Å. The bond length of Cu1–N2 (1.937 Å) is the smallest indicating the strength of azomethine nitrogen in bonding. It is found that the copper atom is closer to semicarbazone moiety than the acetate group. The Cu–$N_{pyridyl}$ bonds are larger by 0.113 Å than Cu–N_{imine} bonds which show the strength of azomethine nitrogen coordination.

The four coplanar basal atoms show a significant distortion from a square geometry as indicated by the N1–Cu1–O1 bond angle of 158.9(3)°. The deviation of the central copper atom from the basal plane in the direction of the axial oxygen is evident from the bond angles of N2–Cu1–O2#1, 111.7(3) and N1–Cu1–O2#1, 94.2(3). Most of the angles involving the central copper atom are widely different from 90° and 180°, indicating significant distortion from the square pyramidal geometry.

The unit cell-packing diagram of compound **4** viewed along a-axis is given in Fig. 2.

It can be observed that the molecules are packed in a 2-dimensional manner with the parallel arrangement of the rings. The adjacent units are interconnected through hydrogen bonding interactions involving the oxygen atom of the acetate group and N^4 hydrogen. The molecular structure pointing up the hydrogen bonding in compound **4** is shown in Fig. 3.

The intermolecular hydrogen bonding interactions are shown in Table 4. The hydrogen-bonding interactions are observed between H4′ of the N4 atom and O3 and between H4A of the O4 atom and O3 with donor-acceptor distances of 2.9939 Å and 2.9347 Å respectively. In addition to this, it also has a non-classical intramolecular hydrogen bond between H3 of the C3 and O1 with a donor-acceptor distance of 2.9625 Å (Table 3). The π-π stacking interactions between metal chelate rings and the aromatic π-π interactions between phenyl and pyridyl ring with Cg-Cg distances of 3.3897 and 3.7215 Å respectively (sym. code: 1-y,1-y,1-z) reinforce crystal structure cohesion in molecular packing in the crystal lattice as shown in Fig. 4. The π–π and intermolecular hydrogen bonding interactions play an important role in the stabilization of the unit cell [36].

The trigonality index τ is calculated using the equation $\tau = (\beta\text{-}\alpha)/60$ [37] (for perfect square pyramidal and trigonal bipyramidal geometries the values of τ are zero and unity respectively). The value of τ for this molecule is 0.187, which again confirms the distorted square pyramidal geometry around the copper atom.

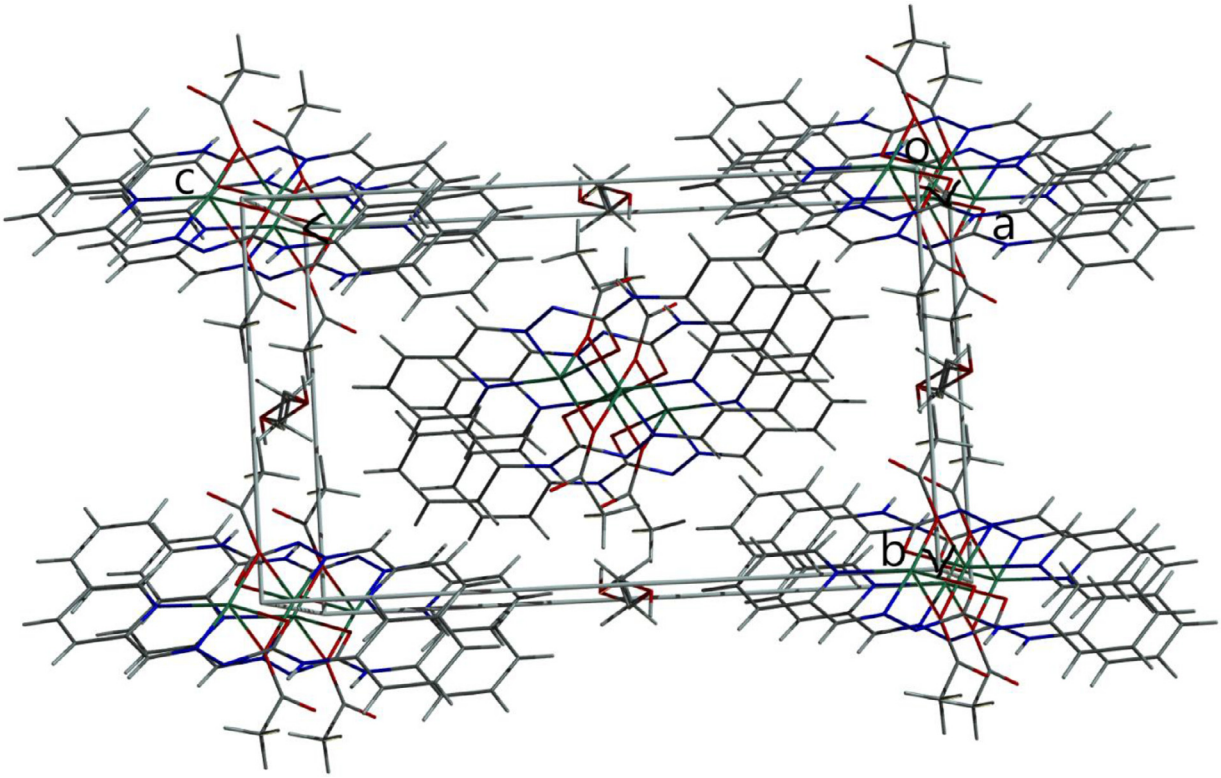

Fig. 2. Packing diagram of compound **4** along 'a' axis.

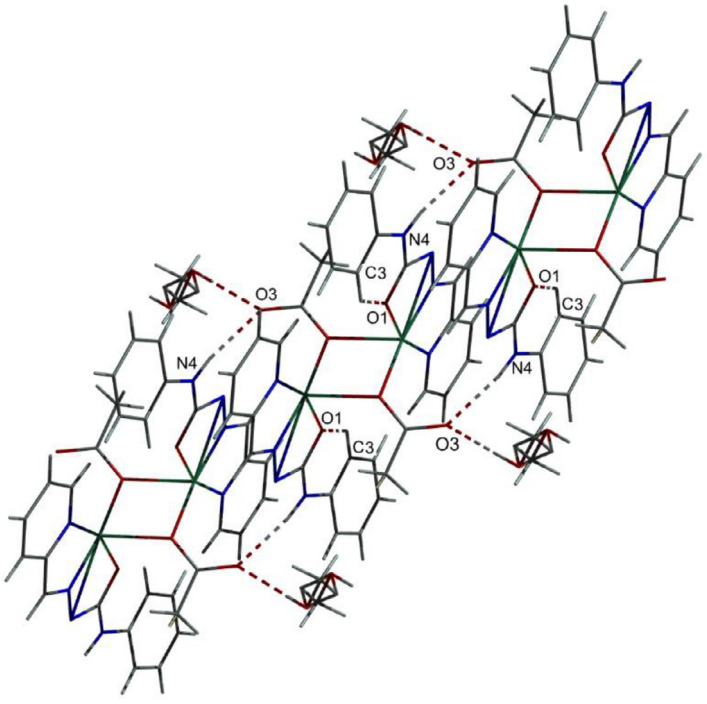

Fig. 3. Packing diagram of compound **4** showing hydrogen bonding.

3.3. Electronic spectra

The significant electronic absorption bands in the spectra of the semicarbazone and all the complexes recorded in methanol and DMF solutions are presented in Table 4.

The semicarbazone and copper(II) complexes have two bands; one centered in the 223-262 nm region and the other in 301-312 nm region. These bands are assigned to $\pi \rightarrow \pi^*$ and $n \rightarrow \pi^*$ transitions (Fig. S1) of phenyl rings and semicarbazone moiety respectively [3,38]. The charge transfer bands were observed in the 405-382 nm region (Table 4) and its broadness can be explained as due to the combination of O→Cu and N→Cu LMCT transitions [39,40].

The $n \rightarrow \pi^*$ and $\pi \rightarrow \pi^*$ transition bands of the uncomplexed semicarbazone are slightly shifted on complexation. This is an in-

Table 3
Interaction parameters of compound 4.

Hydrogen bonding interactions				
D–H···A	D–H (Å)	H···A (Å)	D···A (Å)	∠D–H···A(°)
N(4)–H(4′)···O(3) #2	0.86	2.15	2.9939(10)	168.7
O(4)–H(4A)···O(3)	0.82	2.12	2.93(4)	178.0
C(3)–H(3)···O(1)	0.93	2.42	2.9623(15)	116.9
[$\pi\cdots\pi$ Interactions]				
Cg(I)···Cg(J)	Cg–Cg(Å)	α (°)	β (°)	γ(°)
Cg(2)···Cg(2)[a]	3.389(5)	0.00	16.64	16.64
Cg(4)···Cg(5)[a]	3.721(7)	11.402	22.88	16.59

#2=- -x+1,-y+1,-z+1.
Cg(2) = Cu(1), O(1), C(1), N(3), N(1).
Cg(4) = N(2), C(9), C(10), C(11), C(12), C(13).
Cg(5) = C(2), C(3), C(4), C(5), C(6), C(7).
Equivalent position codes: a = 1-y,1-y,1-z.
D, donor; A, acceptor; Cg, centroid; α, dihedral angles between planes I and J; β, angle between Cg–Cg and Cg(J)_perp; γ, angle between Cg–Cg and Cg(I)_perp.

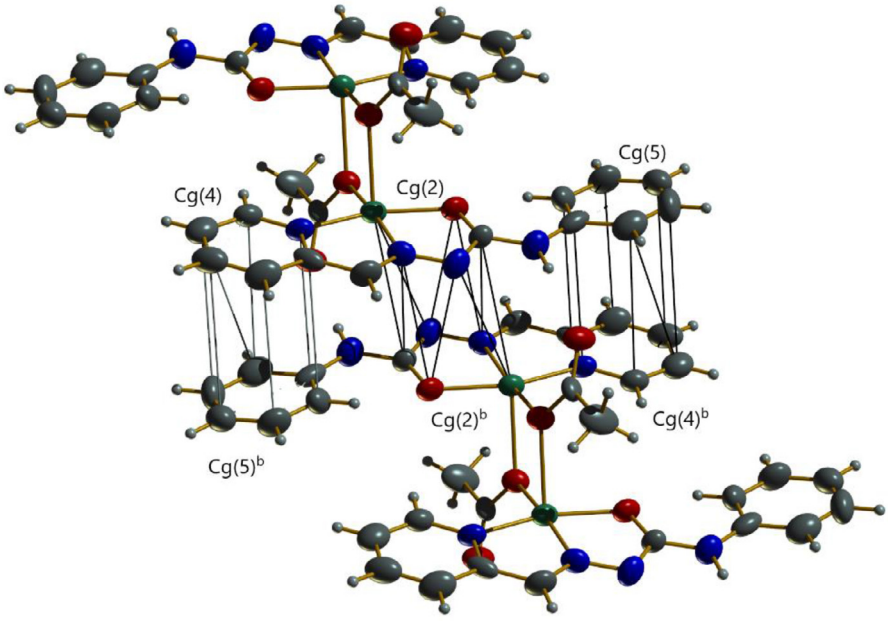

Fig. 4. Crystal structure showing π–π interactions.

Table 4
Electronic spectral assignments (nm) for HPySc and its copper(II) complexes.

Compound	d-d	LMCT	n →π^*	$\pi\rightarrow\pi^*$
HPySc	-	-	312	262, 235
[Cu(HPySc)Cl_2] (**1**)	833	396	305	248
[Cu_2(PySc)$_2$(NO_3)$_2$]·H_2O (**2**)	793, 675	396	304	249
[Cu(HPySc) (SO_4)]·½ H_2O (**3**)	782, 725, 680	396	305	249
[Cu_2(PySc)$_2$($OAc)_2$]·CH_3OH (**4**)	760, 704	405	308	250, 223
[Cu_2(PySc)$_2Br_2$]·H_2O (**5**)	755	398	303	250, 226
[Cu(PySc) (NCS)]·$2H_2O$ (**6**)	704	396	302	250, 226
[Cu_2(PySc)$_2$($N_3)_2$] (**7**)	645	397	301	250, 227

ν.

dication of the coordination of imine nitrogen and amido oxygen to the copper atom.

The spectra of all the complexes exhibit d-d bands in the range of 645 to 833 nm. For a square planar complex with $d_{x^2-y^2}$ ground state, three transitions are possible *viz*, $d_{x^2-y^2}\rightarrow$ d_{xy}, $d_{x^2-y^2}\rightarrow d_{z^2}$ and $d_{x^2-y^2}\rightarrow$ d_{xz}, d_{yz} ($^2B_{2g}\leftarrow$ $^2B_{1g}$, $^2A_{1g}\leftarrow$ $^2B_{1g}$, and ^2E_g $\leftarrow$$^2B_{1g}$) and square pyramidal complexes have the transitions of $d_{x^2-y^2}\rightarrow d_{z^2}$, $d_{x^2-y^2}\rightarrow d_{xy}$ and $d_{x^2-y^2}\rightarrow d_{xz}$, d_{yz} [40]. Complex **6** is expected to be square planar while the other complexes are expected to be a square pyramidal arrangement, among these, complex **4** has been proved to have distorted square pyramidal geometry by the single crystal XRD study. However, since the four *d* orbitals lie very close together, each transition cannot be expected to be distinguished by their energy in all complexes and hence it is very difficult to resolve the bands into separate components. The broadband observed at 833, 755, 704 and 645 nm in the electronic spectra of the complexes **1, 5, 6** and **7** are respectively assigned to $^2E_g\leftarrow$ $^2T_{2g}$ transition [41]. However, complex **3** showed three distinct bands at 782, 725 and 680 nm may be assigned to $^2A_{1g}\leftarrow$ $^2B_{1g}$, $^2B_{2g}\leftarrow$ $^2B_{1g}$ and ^2E_g $\leftarrow$$^2B_{1g}$ respectively. The complexes **2** and **4** gave two distinct bands for each may be assigned to the $^2A_{1g}\leftarrow$ $^2B_{1g}$ and $^2B_{2g}\leftarrow$ $^2B_{1g}$ transitions.

3.4. Infrared spectra

The tentative assignments for the IR spectral bands, most useful for determining the ligand's mode of coordination are listed

Table 5
IR spectral assignments (cm^{-1}) for HPySc and its copper(II) complexes.

Compound	ν(C=N)	ν(N-N)	ν(C=O)	ν(Cu-N)	ν(C=N)[a]	ν(Cu-O)
HPySc	1597	1142	1693	-	-	-
$[Cu(HPySc)Cl_2]$ (**1**)	1587	1168	1647	416	-	468
$[Cu_2(PySc)_2(NO_3)_2]\cdot H_2O$ (**2**)	1593	1148	-	420	1543	498
$[Cu(HPySc)\ (SO_4)]\cdot$ ½ H_2O (**3**)	1593	1164	1645	423	-	474
$[Cu_2(PySc)_2(OAc)_2]\cdot CH_3OH$ (**4**)	1587	1147	-	417	1579	497
$[Cu_2(PySc)_2Br_2]\cdot H_2O$ (**5**)	1589	1160	-	410	1568	468
$[Cu(PySc)(NCS)]\cdot 2H_2O$ (**6**)	1593	1148	-	410	1561	474
$[Cu_2(PySc)_2(N_3)_2]$ (**7**)	1590	1148	-	410	1561	481

[a] Newly formed C=N stretching frequency during complexation.

in Table 5. A sharp band at 1592 cm^{-1} in the ligand can be attributed to the characteristic >C=N group. This band shifts slightly (5-40 cm^{-1}) towards higher frequency in the copper(II) complexes [42] indicating the coordination of azomethine nitrogen to copper(II). It is further supported by the appearance of new bands at 410-423 cm^{-1} assignable to ν(Cu–N) for these complexes [43]. The increase in ν(N–N) values in the spectra of these complexes are due to the increase in double-bond character, off-setting the loss of electron density *via* donation to the metal and is a confirmation of the coordination of the ligand through the azomethine nitrogen. The appearance of bands in the 1543-1579 cm^{-1} range in complexes is due to the asymmetric stretching vibration of the newly formed C=N bond as a result of the enolization of the ligand. The ν(N–H) band of semicarbazone is not distinguishable because of the presence of the broad O–H stretching vibrations in most of the complexes except in $[Cu(HPySc)Cl_2]$ (**1**), $[Cu_2(PySc)_{2(}OAc)_2]\cdot CH_3OH$ (**4**) and $[Cu_2(PySc)_2(N_3)_2]$ (**7**). The disappearance of intense bands of C=O stretching vibrations of semicarbazone complexes **1** and **3** indicates the enolization of the semicarbazone during complexation (Figs S2 & S3). This is further supported by the appearance of a new peak in the 455-498 cm^{-1} range (Table 5) indicating ν(Cu-O) [44].

The appearance of new sharp intense bands at 2115 cm^{-1} and 2045 cm^{-1} are due to the presence of NCS and N_3 groups in complexes **6** and **7** respectively (Figs S4 & S5). Broad bands at 3420-3460 cm^{-1} are due to the presence of lattice water or methanol in the complexes except the complexes **1, 4** and **7**.

Thus, it is seen that the ligand HPySc acts as a monoanionic tridentate ligand in complexes **2, 4, 5, 6**, and **7** whereas, in complexes **1** and **3**, it acts as a neutral tridentate ligand. The sulfato complex $[Cu(HPySc)SO_4]\cdot$½ H_2O has bands at 997, 1039 and 1119 cm^{-1} indicating the presence of bidentate bridging sulfato group [45].

Asymmetric stretching frequencies of unidentate acetato moiety at 1571 and 1565 cm^{-1} and its symmetric stretching frequencies at 1373 and 1365 cm^{-1} is clear evidence for the existence of the monodentate bridging acetate moiety in complex **4** [46]. The peaks are clearly shown in Fig. 5.

Here the complex **6** (Fig S4) exhibits strong and sharp bands at 2115, 748 cm^{-1} and several bands of low intensity near 421 cm^{-1} which can be attributed to ν(CN), ν(CS) and δ(NCS). These values are typical for S-bonded thiocyanato complexes [47].

The azido complex **7** (S5) shows a sharp band at 2040 cm^{-1} and another one at 1243 cm^{-1}. These are assigned to ν_a and ν_s of the coordinated azido group. The broad band observed at 647 cm^{-1} for the complex is assigned to δ(N-N-N) [47]

3.5. Thermal studies

Thermal analyses provide valuable information regarding the thermal stability and nature of water molecules in complexes obtained. It helps to distinguish the lattice water molecules present in the compound. Reports show that the weight losses for lattice water/methanol are in the range of 90–160 °C [47,48]. In complexes **2, 3, 5** and **6,** there are weight losses found in the region 100–160 °C indicate the presence of lattice water molecules. The percentage weight losses of 2.4%, 2.2%, 3.7% and 8.3% respectively agree well with the calculated values indicating the presence of water molecules (Figs S6-S9). . The weight loss of the methanol for **4** fall in the range 200–280 °C (Fig S10).

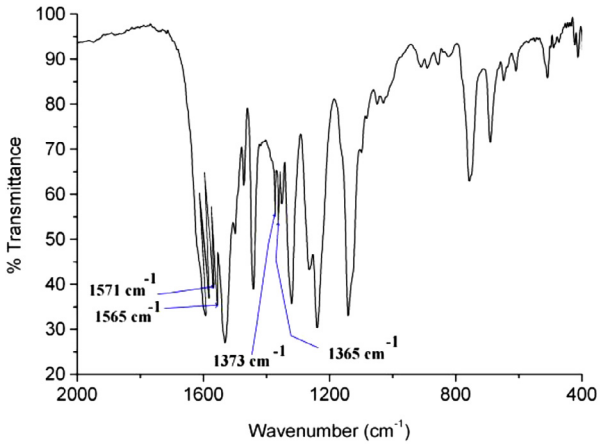

Fig. 5. IR spectrum of complex **4**.

In compounds **1** and **7**, there is no weight loss in this region indicating the absence of solvent molecules (Fig S11 & S12). Complexes **1** and **5** decompose in the temperature range of 220–600 °C while other complexes do in the range of 220-1000 °C which corresponds to the formation of CuO.

3.6. EPR spectra

The EPR spectra of the polycrystalline samples at 298 K, DMF solution at 77 K were recorded in the X-band, using 100-kHz modulation. The EPR parameters $g_{||}$, $g_{\perp}$, $A_{||}$(Cu) and the energies of d-d transitions were used to evaluate the bonding parameters α, β and γ^2 which may be regarded as measures of the covalency in the in-plane σ-bonds, in-plane π-bonds and out-of-plane π-bonds. The value of in-plane σ-bonding parameter α estimated from the expression [49].

$$a^2 = -A_{||}/0.036 + \left(g_{||} - 2.0023\right) + 3/7(g_{\perp} - 2.0023) + 0.04.$$

The following simplified parameters were used to evaluate the bonding parameters [50],

$$K_{||}^2 = (-2.0023)E_{d-d}/8\lambda_o$$

$$K_{\perp}^2 = (g_{\perp} - 2.0023)E_{d-d}/2\lambda_o$$

Where $K_{||} = \alpha^2\ \beta^2$ and $K_{\perp} = \alpha^2\ \gamma^2$, $K_{||}$ and $K_{\perp}$ are orbital reduction factors and λ_0 represents the one-electron spin orbit coupling constant which equals -828 cm^{-1}.

Table 6
Spin Hamiltonian and bonding parameters of copper(II) complexes.

Parameters	Complex						
	1	2	3	4	5	6	7
				Polycrystalline state at 298 K			
$g_{\|}/g_3$	2.273	-	2.290	2.250	2.090	2.240	-
$g_{\perp}/g_2,g_1$	2.054	-	2.075	2.120, 2.058	2.220	2.060	-
g_{iso}/g_{av}	2.127	-	2.146	2.142	2.176	2.120	2.128
G	5.235	-	4.094	2.856	-	4.119	-
				Solution state at 77 K			
$g_{\|}$	2.267	2.274	2.287	2.284	2.278	2.257	2.235
$g_{\perp}$	2.089	2.060	2.079	2.042	2.084	2.077	2.113
$A_{\|}$ (MHz)	440	519	367	695	356	468	485
α^2	0.832	0.862	0.913	1.176	0.907	0.824	0.830
β^2	0.866	0.876	1.127	0.744	1.000	0.895	0.898
γ^2	0.981	0.845	1.307	0.543	1.147	1.109	1.24
$K_{\|}$	0.719	0.757	1.030	0.875	0.908	0.738	0.737
$K_{\perp}$	0.815	0.730	1.195	0.639	1.042	0.915	1.017

The EPR spectra of the compound **7** in the polycrystalline state at 298 K show only one broad signal at $g_{iso} = 2.128$. Such isotropic spectrum (Table 6), consisting of only one broad signal and hence only one g value (g_{iso}), arises from extensive exchange coupling through misalignment of the local molecular axes between different molecules in the unit cell (dipolar broadening) and enhanced spin-lattice relaxation [51]. This type of spectrum unfortunately gives no information on the electronic ground state of copper(II) ions present in the complex.

The spectra of the compounds, **1**, **3** and **6** (Figs S13-S15) in polycrystalline state at 298 K showed axial spectra with well-defined $g_{||}$ and $g_{\perp}$ features. The variation in the $g_{||}$ and $g_{\perp}$ values indicate that the geometry of the compounds in the solid-state is affected by the nature of coordinating anions. For these complexes, the $g_{||} > g_{\perp} > 2.0023$ and the G values are greater than 4 which is consistent with a $d_{x^2-y^2}$ ground state in a square planar or square pyramidal geometry. The geometric parameter G which is a measure of the exchange interaction between copper centers in the polycrystalline compound is calculated using the equation, $G = (g_{||} - 2.0023)/(g_{\perp} - 2.0023)$. G values < 4, are having small exchange coupling interaction [51]. If G>4, exchange interaction is negligible [51,52].

Complex **1** shows negligible exchange interaction and confirms the monomeric nature of the complex while complex **4** gives a G value of 2.856 again as evidence of the dimeric nature of the complex which has been clearly described by the single crystal XRD above. The EPR spectrum of the complex **4** (Fig. S16) in the polycrystalline state shows a rhombic symmetry with three 'g' values suggests that it has a distorted square pyramidal structure.

The spectrum of complex **5** is reverse axial (Fig. S17) in polycrystalline state at 298 K with well-defined $g_{||}$ and $g_{\perp}$ features and the $g_{\perp} > g_{||}$. The $g_{||}$ is found to be 2.090 and $g_{\perp}$ is 2.220. Its dimeric behavior is supported by the magnetic susceptibility (1.186 BM) of the complex.

The absence of signal of the complex **2** in the polycrystalline state may be due to the strong exchange interaction between the copper atoms in the molecule suggesting a dimer for this complex. The magnetic susceptibility value of this complex (1.037 BM) also adds more confidence to our assumption in this regard.

In the EPR spectrum of five-coordinate copper(II) complex **2** in frozen DMF**,** the four fairly resolved hyperfine lines [^{63,65}Cu, $I = 3/2$]. In addition to this, the expected five superhyperfine lines of the two coordinated N atoms (one azomethine nitrogen and the other from pyridyl ring) are also observed in the $g_{||}$ region (Fig. 6). As $g_{||} > g_{\perp}$, a square pyramidal geometry can be assigned and rules out the possibility of a trigonal bipyramidal structure which would be expected to have $g_{\perp} > g_{||}$. The α^2, β^2 and γ^2 values of this

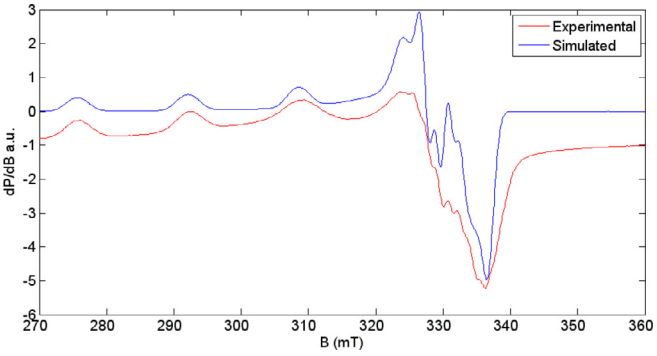

Fig. 6. EPR spectrum of complex **2** in DMF at 77 K.

complex are less than one and indicate that the complexes are consistent with both strong in-plane σ-bonding and in-plane π-bonding. The orbital reduction factor $K_{||} < K_{\perp}$ also support that the complex involved in in-plane π-bonding [53].

The EPR spectra of the five-coordinate copper(II) complexes **4** and **7** in DMF at 77 K show resolved four copper hyperfine lines (Figs S18 & S19). The expected superhyperfine splittings of nitrogen atoms are not observed. The $g_{||} > g_{\perp}$ suggests a square pyramidal geometry for these complexes, one of which is proved to have square pyramidal geometry on the basis of SXRD data. The fraction of lone pair electron density on the copper ion is relatively higher (α=1.176 and 0.824 respectively) for complex **4** illustrates that the copper ion engaged with more ionic type bonding with the ligand while the other involved in covalent type bonding.

The complex **5** showed reverse axial spectrum in solid-state and indicates that it has a d_{z^2} ground state with trigonal bipyramidal geometry, however in solution state, it gave an axial spectrum and this may be because of the dissociation of dimeric structure into monomeric in DMF solvent by the involvement of DMF solvent molecule (Fig. S20). The $g_{||}/A_{||}$ ratio of the complex in DMF (168.6) is not in the range (90-140 cm) of a square planar structure [54] confirms the presence of DMF molecule in the complex. The α^2, β^2 and γ^2 parameters (Table 6) of this complex indicating the involvement of more ionic behavior reveals that it has weak in-plane σ- bonding and in-plane π-bonding with the metal ion.

The isotropic/average g values of the complexes **1, 3** and **6** in the polycrystalline state are similar to the average g values in the solution state (Figs S21-S23) suggest that it is not undergoing any kind of dissociation in the solution state. These spectra in DMF/DMSO at 77 K did not give the expected superhyperfine lines. However, they show well defined four-line hyperfine splitting of

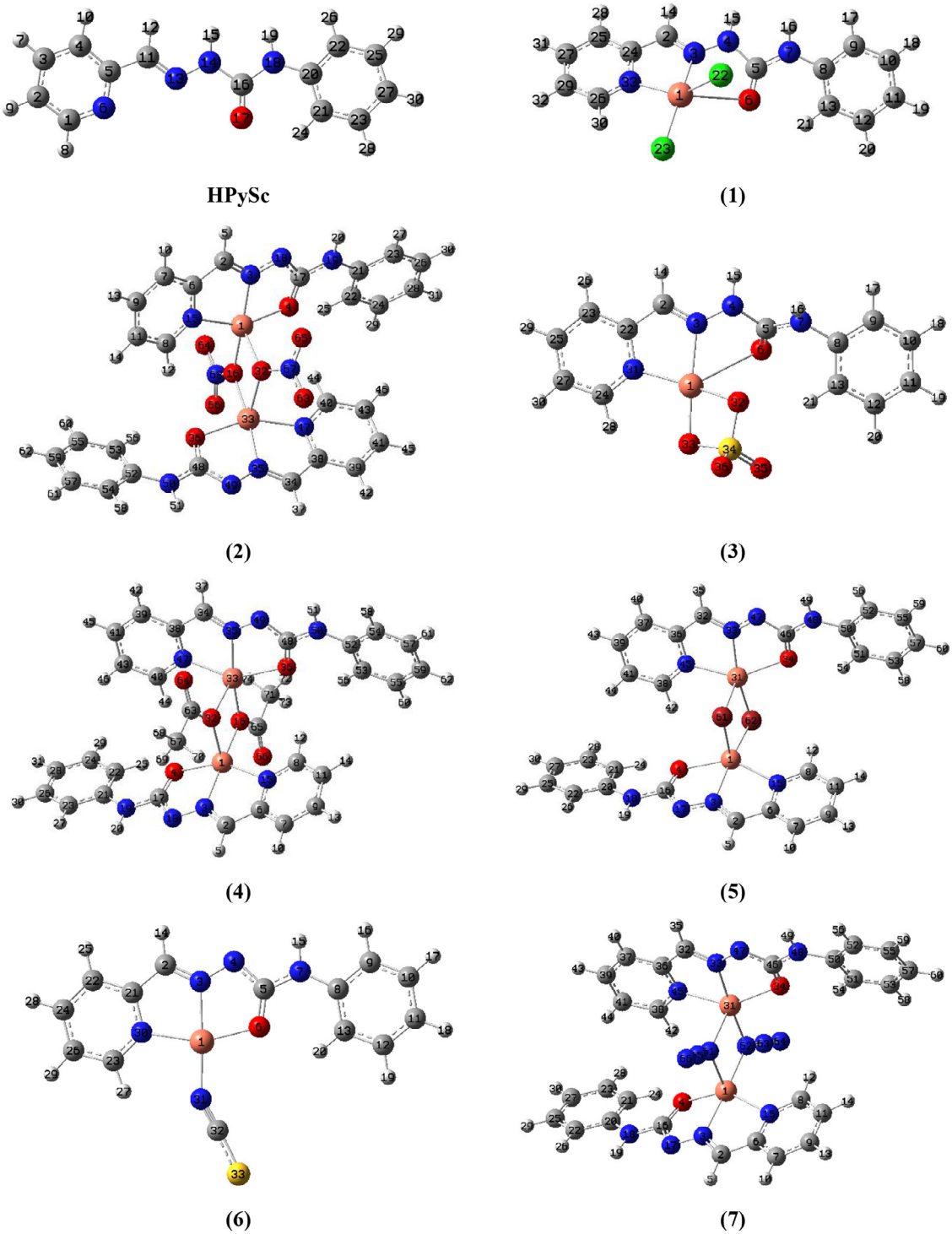

Fig. 7. The optimized geometries of the HPySc and seven Cu(II) complexes at RB3LYP/6-311G(d,p)/LANL2DZ.

copper. The $g_{||}$ /$A_{||}$ ratio of the complexes **1** and **6** are 136 and 128 respectively suggests a square planar geometry while the other lies out of the range of the square planar geometry (90-140 cm^{-1}) indicating square pyramidal coordination around the metal atom since its ground state orbital is still $d_{x^2-y^2}$. The α^2, β^2 and γ^2 parameters of these complexes provide the information that the metal-ligand bonds are more covalent in nature than the other complexes and the $K_{||} < K_{\perp}$ also point out that these complexes have strong in-plane σ-boning and in-plane π-bonding.

3.7. DFT calculations

3.7.1. Natural bond orbitals

Nowadays, NBO computations have been used in a lot of different molecular systems to provide useful information on possible donor-acceptor interactions [55–58]. Here, the optimized structures of ligand HPySc and Cu(II) complexes **1-7** are given in Fig. 7. Also, the NBO analyzes results of all studied compounds are given in Tables S1-S8.

Table 7
The physicochemical and quantum chemical quantities of the HPySc and seven Cu(II) complexes at RB3LYP/6-311G(d,p)/LANL2DZ.

	HPySc	1	2	3	4	5	6	7
H (-I) (eV)	-6.015	-6.614	-5.556	-6.501	-5.369	-5.347	-5.906	-5.421
L (-A) (eV)	-1.745	-3.113	-4.764	-3.420	-4.515	-4.680	-2.915	-4.572
ΔE (L-H) (eV)	4.269	3.502	0.792	3.081	0.853	0.667	2.991	0.848
μ (eV)	-3.880	-4.863	-5.160	-4.961	-4.942	-5.013	-4.411	-4.996
η (eV)	2.135	1.751	0.396	1.540	0.427	0.333	1.496	0.424
ω (eV)	0.130	0.248	1.235	0.294	1.052	1.385	0.239	1.081
ω^+ (au)	0.068	0.167	1.142	0.209	0.963	1.295	0.165	0.991
ω^- (au)	0.211	0.346	1.331	0.392	1.144	1.479	0.327	1.175
ΔN_{max} (eV)	1.817	2.778	13.023	3.220	11.582	15.040	2.949	11.777
$\Delta E_{back.}$ (eV)	-0.534	-0.438	-0.099	-0.385	-0.107	-0.083	-0.374	-0.106
DM (D)	6.101	13.600	1.267	16.742	1.187	1.440	9.486	1.748
α (au)	199.719	255.181	675.609	241.885	665.293	739.173	310.117	676.170

For the ligand HpySc, the interactions LP (1) N14 → Π* C11–N13 ($E^{(2)}$= 31.70 kcal/mol), LP (1) N14 → Π* C16–O17 ($E^{(2)}$= 44.07 kcal/mol), LP (1) N18 → Π* C16-O17 ($E^{(2)}$= 53.41 kcal/mol), and LP (1) N18 → Π* C20–C21 ($E^{(2)}$= 32.58 kcal/mol) had great role in the lowering the stabilization. In the presence of the Cu(II) atom, the corresponding interactions for complex **1** are determined as LP (1) N4 → Π* C2–N3 ($E^{(2)}$= 16.37 kcal/mol), LP (1) N4 → Π* C5–O6 ($E^{(2)}$= 14.64 kcal/mol), LP (1) N7 → Π* C5–O6 ($E^{(2)}$= 28.10 kcal/mol), and LP (1) N7 → Π* C8–C9 ($E^{(2)}$= 13.82 kcal/mol), which are lower than those of the free ligand. Besides, the LP (1) N3 → LP* (6) Cu1 interaction for complex **1** is calculated with an energy of 6.62 kcal/mol. The interaction LP (1) N7 → Π* C5–O6 for complex **3** is calculated with the stabilization energy of 30.13 kcal/mol that is the greatest contribution. Besides, the electron movement to Cu–O bridge from each LP (1) 3 and LP (1) N31 are calculated for the anomeric interactions LP (1) N3 → σ^* Cu1–O33 ($E^{(2)}$= 10.41 kcal/mol) and LP (1) N31 → σ^* Cu1–O32 ($E^{(2)}$= 11.73 kcal/mol) (Table S4). For complex **3**, the remaining anomeric interactions had sourced by the electron movement over the sulfato group linked to Cu(II), which are as LP (3) O35 → σ^* O33–S34 ($E^{(2)}$= 10.27 kcal/mol) and LP (3) O36 → σ^* O32–S34 ($E^{(2)}$= 10.47 kcal/mol). For the complex **6**, it can be noticed from Table S7 that the isothiocyanate (–NCS) group has the greatest role in decreasing the stabilization energy, contributed by the interactions σ Cu1–S33 (1) → Π* N31–C32 ($E^{(2)}$= 35.50 kcal/mol) and LP (2) S33 → Π* N31–C32 ($E^{(2)}$= 29.19 kcal/mol).

For complex **2**, the interactions LP (1) N19 → Π* C17–N18 ($E^{(2)}$= 60.36 kcal/mol) and LP (1) N50 → Π* C48–N49 ($E^{(2)}$= 59.90 kcal/mol) significantly contributed to energy lowering of the complex. Moreover, the charge movement to unoccupied *d*-orbital of Cu(II) atom from the nitrogen of the pyridine ring made a decrease in the energy of complex **2**, significantly. In this respect, the relevant interactions between the nitrogen atom and Cu(II) atom are determined as LP (1) N15 → LP* (6) Cu1 ($E^{(2)}$= 24.26 kcal/mol), LP (1) N47 → LP* (6) Cu33 ($E^{(2)}$= 28.39 kcal/mol. Furthermore, the electron flowing over the Cu–O–Cu linkage is remarkable. Namely, the energy lowering for the electron movement to unfilled orbitals LP* (6) Cu1 and LP* (6) Cu33 from the lone pair of O16 atom is calculated as 9.41 and 9.67 kcal/mol (Table S3). From Table S3, the electrons of the oxygen atom in the bridge of Cu–O–Cu are calculated more likely to be delocalized on the nitro group that is determined as LP (2) O16 → σ^* O64–N68 (E(2)= 48.36 kcal/mol). The biggest energy interactions for complex **4** are determined as LP (1) N19→ Π* C17–N18 ($E^{(2)}$= 58.98 kcal/mol), LP (1) N50→ Π* C48–N49 ($E^{(2)}$= 57.98 kcal/mol), and LP (2) O16→ Π* C65–O66 ($E^{(2)}$= 47.43 kcal/mol). Besides, the electron donation to each Cu atom from the oxygens contributed to stabilization of complex **4** and are determined as LP (2) O4→ LP* (5) Cu1 ($E^{(2)}$= 20.14 kcal/mol), LP (2) O4→ LP* (7) Cu1 ($E^{(2)}$= 19.47 kcal/mol), LP (2) O36→ LP* (6) Cu33 ($E^{(2)}$= 16.52 kcal/mol), and LP (2) O36→ LP* (8) Cu33 ($E^{(2)}$= 22.03 kcal/mol). From Table S6, the corresponding interactions for complex **5** are predicted as: LP (1) O4→ LP* (9) Cu1 ($E^{(2)}$= 16.21 kcal/mol) and LP (1) O34→ LP* (9) Cu31 ($E^{(2)}$= 16.95 kcal/mol). For complex **5**, the electron transfer to Cu atom from each bromine are characterized by the interactions as follows: LP (3) Br61→ LP* (6) Cu1 ($E^{(2)}$= 14.63 kcal/mol), LP (3) Br61→ LP* (6) Cu31 ($E^{(2)}$= 22.42 kcal/mol), LP (4) Br61→ LP* (6) Cu1 ($E^{(2)}$= 34.37 kcal/mol), LP (4) Br61→ LP* (6) Cu31 ($E^{(2)}$= 28.39 kcal/mol), LP (3) Br62→ LP* (6) Cu1 ($E^{(2)}$= 25.01 kcal/mol), and LP (3) Br62→ LP* (6) Cu31 ($E^{(2)}$= 23.86 kcal/mol). The main interactions for complex **7** are determined as LP (1) N18→ Π* C16–N17 ($E^{(2)}$= 57.86 kcal/mol), LP (1) N18→ Π* C20–N21 ($E^{(2)}$= 36.07 kcal/mol), LP (1) N48→ Π* C46–N47 ($E^{(2)}$= 59.04 kcal/mol), and LP (1) N48→ Π* C50–C51 ($E^{(2)}$= 36.03 kcal/mol). Besides, the interactions LP (1) N3→ LP*(7) Cu1 ($E^{(2)}$= 19.57 kcal/mol), LP (1) N15→ LP*(8) Cu1 ($E^{(2)}$= 24.02 kcal/mol), LP (1) N33→ LP*(7) Cu31 ($E^{(2)}$= 18.71 kcal/mol), LP (1) N45→ LP*(8) Cu31 ($E^{(2)}$= 26.33 kcal/mol) contributed to the energy lowering of complex **7**. From these results, it can be said that the charge distributions, polarizations, and ultimately chemical reactivity of complexes **1**-**7** and semicarbazone are evaluated based on intramolecular interactions.

3.7.2. Frontier molecular orbitals

In addition to being used for a long time to elucidate the structure and related properties of organic and simple molecular systems [59,60], QCPs are frequently applied to metal complexes [39,61-63] to determine/verify the structural and spectroscopic properties. In this respect, the determined QCPs for the ligand HPySc and complexes **1**-**7** are given in Table 7.

According to the ΔE_{gap} values, which is determined as HPySc (4.269) > **1** (3.502) > **3** (3.081) > **6** (2.991) > **4** (0.853) > **7** (0.848) > **2** (0.792) > **5** (0.667), the presence of Cu(II) and the substitutions on each complex provided the relevant compound more stable than the ligand. Besides, the μ (eV) order is calculated as HPySc (-3.880) > **6** (-4.411) > **1** (-4.863) > **4** (-4.942) > **3** (-4.961) > **7** (-4.996) > **5** (-5.013) > **2** (-5.160) and pointed out that the complex **2** is the most electronically stable among the complexes. Furthermore, the ligand HPySc is the hardest and complex **5** is the softer than all complexes due to the η (eV) values are in the following order: HPySc (2.135) > **1** (1.751) > **3** (1.540) > **6** (1.496) > **4** (0.427) > **7** (0.424) > **2** (0.396) > **5** (0.333). As expected, the presence of Cu(II) gained to the complex the electrophilic character. Namely, the ω (eV) order is predicted as HPySc (0.130) < **6** (0.239) < **1** (0.248) < **3** (0.294) < **4** (1.052) < **7** (1.081) < **2** (1.235) < **5** (1.385). For all complexes, the electron donating capability are calculated greater than the electron accepting power. Also, the electron donating and electron accepting potencies of the complexes **2, 4, 5**, and **7** linked with two ligands are bigger than that of the ones with one ligated (**1, 3**, and **6**). Besides, the existence of Cu(II) in the complexes provided the charge transfer capability greater in

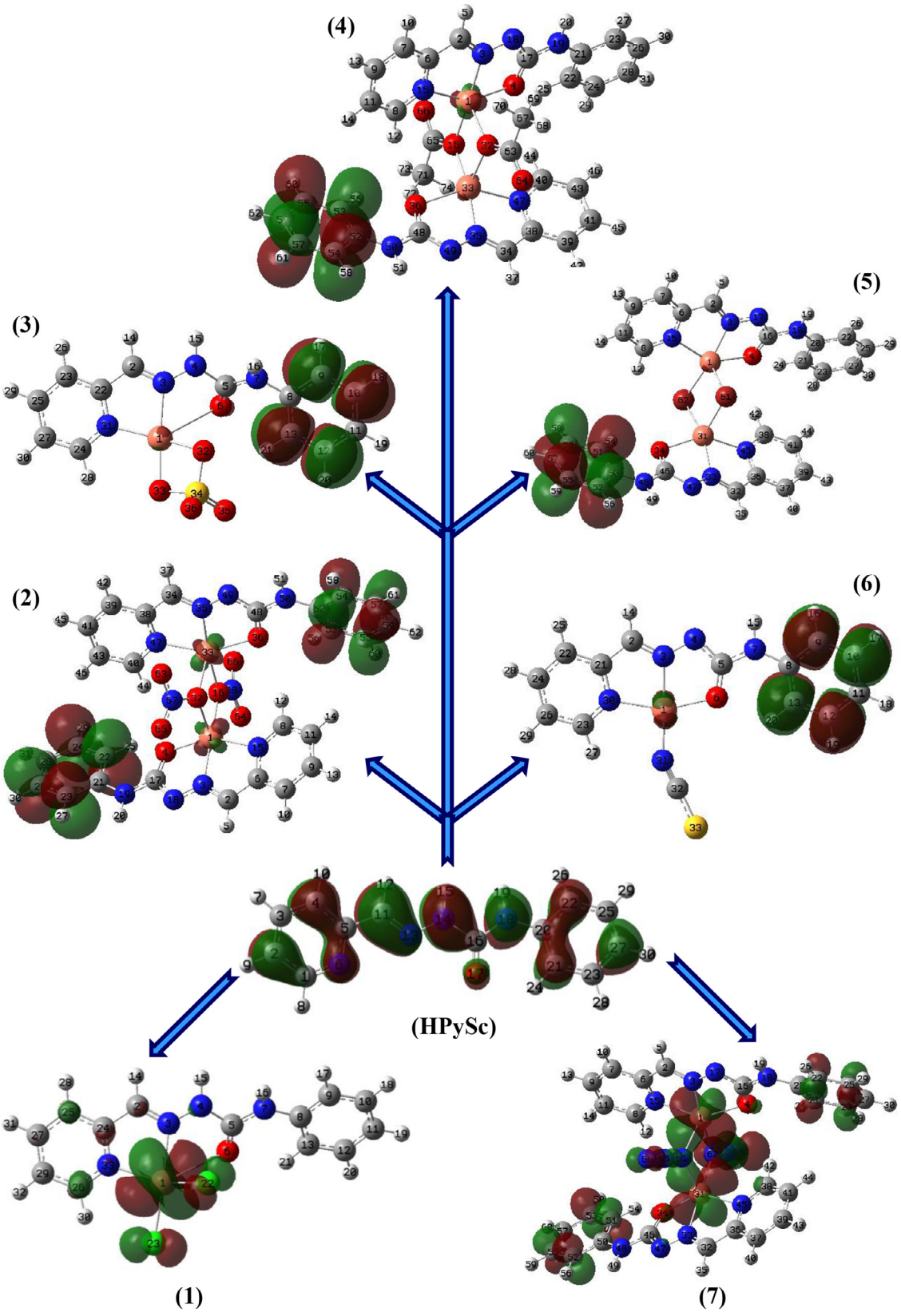

Fig. 8. HOMO (isoval:0.02) density for HPySc and seven Cu(II) complexes at B3LYP/6-311G(d,p)/LANL2DZ.

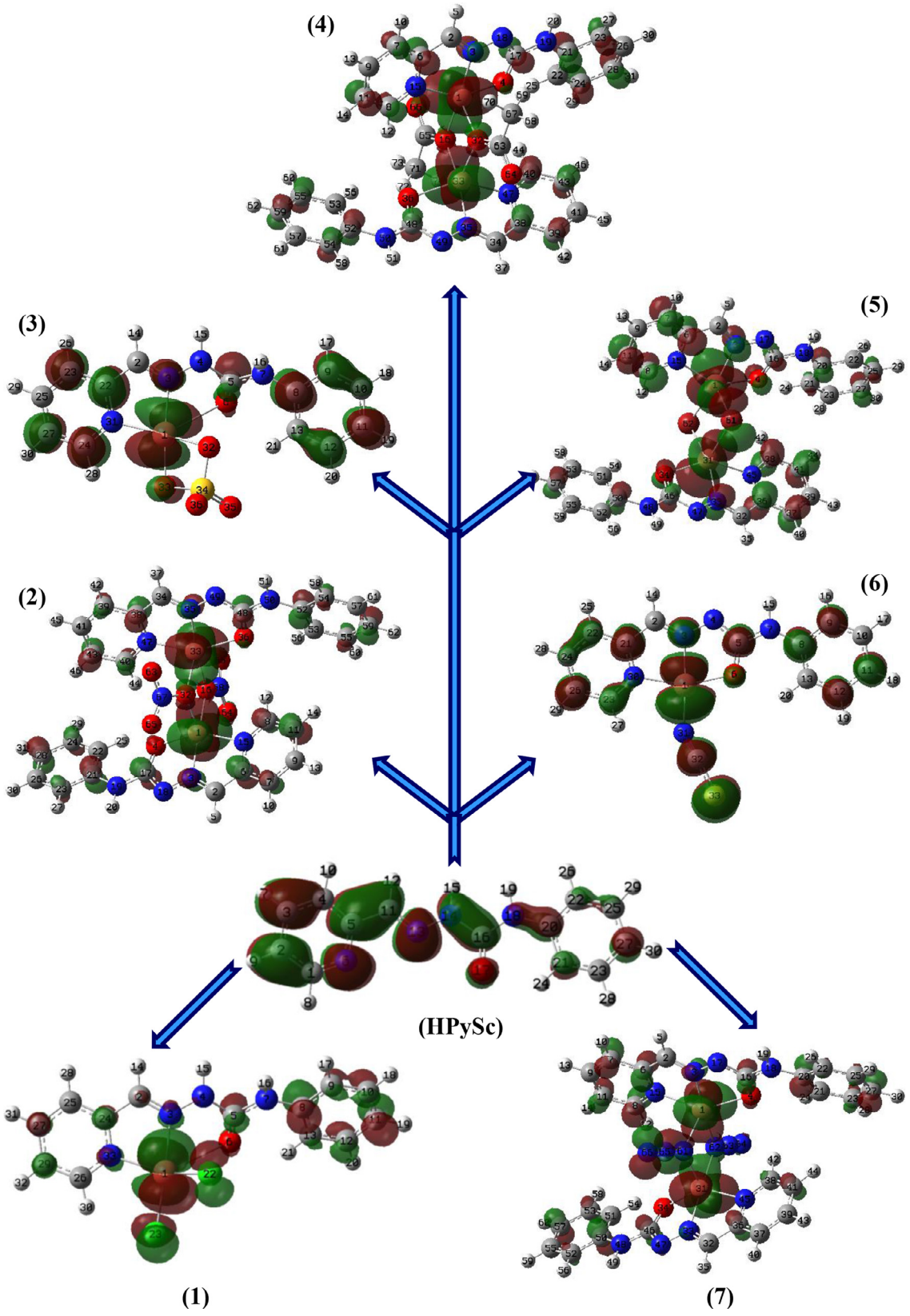

Fig. 9. LUMO (isoval:0.02) density for HPySc and seven Cu(II) complexes at B3LYP/6-311G(d,p)/LANL2DZ.

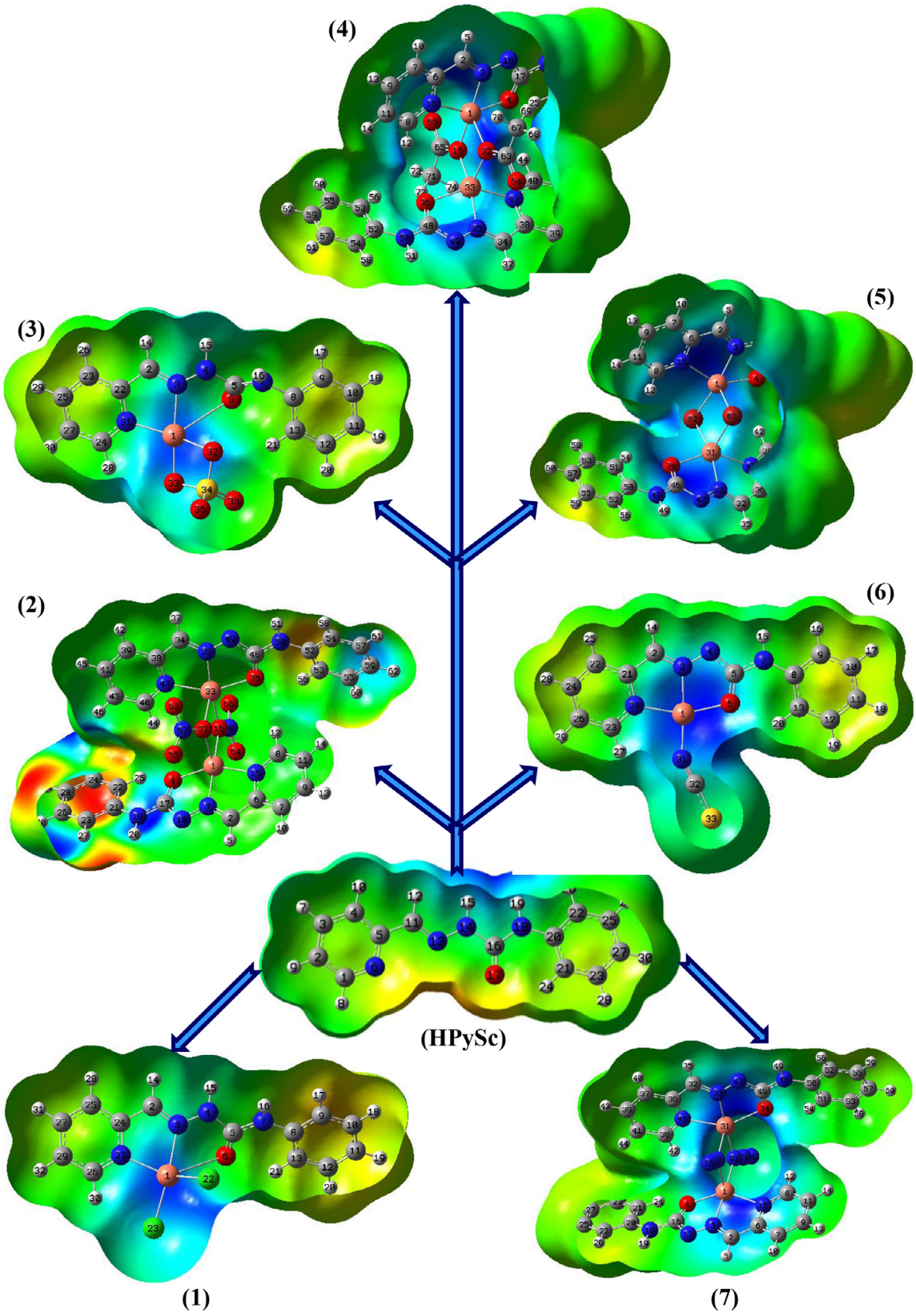

Fig. 10. MEP (isoval:0.0004) for HPySc and seven Cu(II) complexes at B3LYP/6-311G(d,p)/LANL2DZ.

comparison to the ligand. The ΔN_{max} value (Table 7) of bis ligated complexes **2** (13.023 eV), **4** (11.582 eV), **5** (15.040 eV), and **7** (11.777 eV) are significantly bigger than the mono-ligated complexes **1** (2.778 eV), **3** (3.220 eV), and **6** (2.949 eV). As expected, the back-donation energies of complexes **1** (-0.438 eV), **3** (-0.385 eV), and **6** (-0.374 eV) are calculated to be greater than the complexes **2** (-0.099 eV), **4** (-0.107 eV), **5** (-0.083 eV), and **7** (-0.106 eV). In agreement mainly with the MHP (maximum hardness principle) and MPP (minimum polarizability principle) [64–67], the polarizability values of all compounds are calculated as HPySc (199.719) < **3** (241.885) < **1** (255.181) < **6** (310.117) < **4** (665.293) < **2** (675.609) < **7** (676.170) < **5** (739.173).

In addition, the HOMO, LUMO, and MEP graphs for the ligand HPySc and complexes **1**-**7** are presented in Fig. 8, Fig. 9, and Fig. 10, respectively. For the ligand HPySc, the HOMO as a sign of the nucleophilic attack region expanded on the whole surface of the molecule. Furthermore, the HOMOs for complexes **2**-**6** are distributed only on their phenyl rings, whereas the HOMO for complex **1** spread out on Cl–Cu–Cl. The HOMO density for complex **7** appeared greatly on two Cu centers linked with the N_3 fragment and partially on the phenyl ring. For the HPySc, the LUMO density as a sign of the electrophilic attacks spread on the whole surface except for the phenyl ring, whereas the LUMOs for all complexes mainly enlarged around Cu. For complexes **2, 4, 5**, and **7**, the LUMOs partially expanded on the PySc unit (Fig. 9), whereas the LUMOs of complexes **3** and **6** distributed on the whole surface except for the -SO_3 group and nitrogens. From Fig. 10, the oxygen and H atoms bonded nitrogen atom of the semicarbazone HPySc are covered by red (V< 0) and blue (V> 0) colors. In the MEP plots, the electron density on the surface has expressed by the color scheme as a function of the electrostatic potential. Accordingly, the red color shows the electron-rich site for electrophilic attacks whereas the blue color indicates the electron-poor region for nucleophilic attacks. Thus, the surrounding of Cu for all complexes is covered by blue color for the nucleophilic attacks, whereas the phenyl ring for complex **2** is covered by red color to electrophilic attacks.

Conclusion

We have synthesized and characterized seven copper(II) complexes with 2-pyridinecarboxaldehyde-N^4-phenylsemicarbazone (HPySc) and characterized using different analytical and spectroscopic techniques such as FT IR, EPR, electronic spectral studies, thermogravimetric analysis, conductance and magnetic susceptibility measurements and single-crystal XRD studies. Complex **6** is found to be square planar while the other complexes are square pyramidal in nature. The single-crystal XRD study proves that complex **4** is a dimer and copper(II) centers adopt distorted square pyramidal geometry. All the complexes are found to be paramagnetic and non-electrolytic in nature. The semicarbazone ligand is coordinated in the neutral form in two of the complexes and deprotonated form in others. DFT/B3LYP/6-311g**/LANL2DZ computations of the ligand HPySc and seven Cu(II) complexes are performed to analyze the FMOs and important electron delocalizations in the ligand and the complexes. NBO analysis revealed that all the complexes are more stable than the ligand and complex **2** is the most electronically stable and softest compared to all other complexes. The nucleophilic and electrophilic reactivities also are analyzed in terms of the energy gap between HOMO and LUMO energies.

Author contribution

All authors have contributed equally to the manuscript

Supplementary data

CCDC 2131659 contains the supplementary crystallographic data for $[Cu_2(PySc)_2(OAc)_2]\cdot CH_3OH$ (**4**). The data can be obtained free of charge *via* www.ccdc.cam.ac.uk/conts/retrieving.html or from the Cambridge Crystallographic Data Centre, 12 Union Road, Cambridge CB2 IEZ, UK; fax: (+44) 1223-336-033; or e-mail: deposit@ccdc.cam.ac.uk.

Declaration of Competing Interest

The authors declare that they have no known competing financial interests or personal relationships that could have appeared to influence the work reported in this paper.

Data availability

The data is deposited in CCDC

Acknowledgments

The authors are thankful to the SAIF, Cochin University of Science and Technology, Kochi, Kerala, India for elemental analyses and SAIF, IIT, Bombay, India for EPR spectra. M. Sithambaresan is thankful to the Indian Council for Cultural Relations (ICCR), New Delhi, India for a research scholarship (SAARC/HTT/ICCR-India/07). Prof. Mathias Zeller, Department of Chemistry, Purdue University is acknowledged for his help in refining the SXRD data. All quantum chemical calculations were performed at TUBITAK-ULAKBIM, High Performance and Grid Computing Center (TRUBA resources), TURKEY.

Supplementary materials

Supplementary material associated with this article can be found, in the online version, at doi:10.1016/j.molstruc.2022.134866.

References

[1] T.K. Venkatachalam, P.V. Bernhardt, C.J. Noble, N. Fletcher, G.K. Pierens, K.J. Thurecht, D.C. Reutens, Synthesis, characterization and biological activities of semicarbazones and their copper complexes, J. Inorg. Biochem. 162 (2016) 295–308.
[2] C. Boulechfar, H. Ferkous, S. Boufas, M. Berredjem, A. Delimi, S. Djellali, A. Djedouani, R. Bahadi, S. Laamari, K.K. Yadav, B.-H. Jeon, W. Bouchelaghem, M. Alam, Y. Benguerba, Synthesis, electrochemical, and quantum chemical studies of some metal complexes: Mn(II), Co(II), and Zn(II) with 2-furaldehyde semicarbazone, J. Mol. Struct. 1271 (2023) 134007.
[3] U.L. Kala, S. Suma, M.R.P. Kurup, S. Krishnan, R.P. John, Synthesis, spectral characterization and crystal structure of copper(II) complexes of 2-hydroxyacetophenone N(4)-phenyl semicarbazone, Polyhedron 26 (2007) 1427–1435.
[4] T.A. Reena, E.B. Seena, M.R.P. Kurup, Zinc(II) complexes derived from di-2-pyridyl ketone N4-phenyl-3-semicarbazone: crystal structure and spectral studies, Polyhedron 27 (2009) 3461–3466.
[5] C.C. Gatto, F.C. Lima, P.M. Miguel, Copper(II) complexes with semicarbazones: synthesis, characterization and noncovalent interactions in their crystal structures, J. Chem. Sci. 132 (2020) 132–146.
[6] G. Scalese, J. Benitez, S. Rostan, I. Correia, L. Bradford, M. Vieites, L. Minini, A. Merlino, E.L. Coitino, E. Birriel, J. Varela, H. Cerecetto, M. Gonzalez, J.C. Pessoa, D. Gambino, Expanding the family of heteroleptic oxidovanadium(IV) compounds with salicylaldehyde semicarbazones and polypyridyl ligands showing anti-Trypanosoma cruzi activity, J. Inorg. Biochem. 147 (2015) 116–125.
[7] X. Jiang, L. Sheng, C. Song, N. Du, H. Xu, Z. Liu, S. Chen, Mechanism, kinetics, and antimicrobial activities of 2-hydroxy-1-naphthaldehyde semicarbazone as a new Jack bean urease inhibitor, New J. Chem. 40 (2016) 3520–3527.
[8] D. Tómasson, D. Ghosh, M.R.P. Kurup, M.T. Mulvee, K.K. Damodaran, Evaluating the role of urea-like motif in enhancing the thermal and mechanical strength of supramolecular gel, CrystEngComm 23 (2021) 617.
[9] M.M. Roessler, E. Salvadori, Principles and applications of EPR spectroscopy in the chemical sciences, Chem. Soc. Rev. 47 (2018) 2534.
[10] S.F.F. dos Santos, A.A. Oliveira, G.R. Santos, G. Mahmoudi, F.A. Afkhami, P.S. Santiago, R.B. Viana, A.B.F. da Silva, R.H.A. Santos, J. Mol. Struct. 1197 (2019) 393.
[11] M. Sithambaresan, M.R.P. Kurup, Acta Cryst. E67 (2011) o2972.

[12] S. Stoll, A. Schweiger, EasySpin, a comprehensive software package for spectral simulation and analysis in EPR, J. Magn. Reson. 178 (2006) 42–55.
[13] G.M. Sheldrick, Crystal structure refinement with SHELXL, Acta Crystallogr. C71 (2015) 3–8.
[14] K. Brandenburg, Diamond Version 3.2k, Crystal Impact GbR, 2014 Bonn, Germany.
[15] A.D. Becke, A new mixing of Hartree–Fock and local density-functional theories, J. Chem. Phys. 98 (1993) 1372–1377.
[16] C. Lee, W. Yang, R.G. Parr, Development of the Colle-Salvetti correlation-energy formula into a functional of the electron density, Phys. Rev. B37 (1988) 785–789.
[17] P.J. Hay, W.R. Wadt, *Ab initio* effective core potentials for molecular calculations. Potentials for K to Au including the outermost core orbitals, J. Chem. Phys. 82 (1985) 299–310.
[18] R. Ditchfield, W.J. Hehre, J.A. Pople, Self-consistent molecular-orbital methods. IX. An extended Gaussian-type basis for molecular-orbital studies of organic molecules, J. Chem. Phys. 54 (1971) 724–728.
[19] R. Krishnan, J.S. Binkley, R. Seeger, J.A. Pople, J. Chem. Phys. 72 (1980) 650–654.
[20] M.J. Frisch, G.W. Trucks, H.B. Schlegel, G.E. Scuseria, MA. Robb, J.R. Cheeseman, G. Scalmani, V. Barone, B. Mennucci, G.A. Petersson, H. Nakatsuji, M. Caricato, X. Li, H.P. Hratchian, A.F. Izmaylov, J. Bloino, G. Zheng, J.L. Sonnenberg, M. Hada, M. Ehara, K. Toyota, R. Fukuda, J. Hasegawa, M. Ishida, T. Nakajima, Y. Honda, O. Kitao, H. Nakai, T. Vreven, J.A. Montgomery Jr., J.E. Peralta, F. Ogliaro, M. Bearpark, J.J. Heyd, E. Brothers, K.N. Kudin, V.N. Staroverov, T. Keith, R. Kobayashi, J. Normand, K. Raghavachari, A. Rendell, J.C. Burant, S.S. Iyengar, J. Tomasi, M. Cossi, N. Rega, J.M. Millam, M. Klene, J.E. Knox, J.B. Cross, V. Bakken, C. Adamo, J. Jaramillo, R. Gomperts, R.E. Stratmann, O. Yazyev, A.J. Austin, R. Cammi, C. Pomelli, J.W. Ochterski, R.L. Martin, K. Morokuma, V.G. Zakrzewski, G.A. Voth, P. Salvador, J.J. Dannenberg, S. Dapprich, A.D. Daniels, O. Farkas, J.B. Foresman, J.V. Ortiz, J. Cioslowski, D.J. Fox, Gaussian 09W, Revision D.01, Gaussian, Inc, Wallingford CT, 2013.
[21] GaussView 6.0.16, Gaussian, Inc, Wallingford CT, 2016.
[22] T. Koopmans, Uber die Zuordung von Wellenfunktionen und Eigenwertenzu den einzelnen Elektroneneines Atoms, Physica 1 (1934) 104–113.
[23] J.P. Perdew, R.G. Parr, M. Levy, J.L. Balduz, Density-functional theory for fractional particle number: derivative discontinuities of the energy, Phys. Rev. Lett. 49 (23) (1982) 1691–1694.
[24] J.F. Janak, Proof That dEdni $=\varepsilon$ in density-functional theory, Phys. Rev. B. 18 (12) (1978) 7165–7168.
[25] J.P. Perdew, M. Levy, Physical content of the exact Kohn-Sham orbital energies: band gaps and derivative discontinuities, Phys. Rev. Lett 51 (1983) 1884–1887.
[26] R.G. Parr, R.G. Pearson, Absolute hardness: companion parameter to absolute electronegativity, J. Am. Chem. Soc. 105 (1983) 7512–7516.
[27] R.G. Pearson, Absolute electronegativity and hardness correlated with molecular orbital theory, Proc. Natl. Acad. Sci. USA 83 (1986) 8440–8441.
[28] R.G. Parr, L.V. Szentpaly, S. Liu, Electrophilicity index, J. Am. Chem. Soc. 121 (1999) 1922–1924.
[29] J.L. Gazquez, A. Cedillo, A. Vela, Electrodonating and electroaccepting powers, J. Phys. Chem. A 111 (10) (2007) 1966–1970.
[30] B. Gomez, N.V. Likhanova, M.A. Domínguez-Aguilar, R. Martínez-Palou, A. Vela, J.L. Gazquez, Quantum chemical study of the inhibitive properties of 2-pyridyl-azoles, J. Phys. Chem. B 110 (18) (2006) 8928–8934.
[31] J.P. Foster, F. Weinhold, Natural hybrid orbitals, J. Am. Chem. Soc. 102 (1980) 7211–7218.
[32] A.E. Reed, R.B. Weinstock, F. Weinhold, Natural population analysis, J. Chem. Phys. 83 (1985) 735–746.
[33] A.E. Reed, F. Weinhold, J. Natural localized molecular orbitals, Chem. Phys. 83 (1985) 1736–1740.
[34] W.J. Geary, The use of conductivity measurements in organic solvents for the characterisation of coordination compounds, Coord. Chem. Rev. 7 (1971) 81.
[35] M.M. Fousiamol, M. Sithambaresan, K.K. Damodaran, M.R.P. Kurup, Syntheses, spectral aspects and biological studies of bromide and azide bridged box dimer copper(II) complexes of an NNO donor aroylhydrazone, Inorg. Chim. Acta 501 (2020) 119301.
[36] P.F. Rapheal, E. Manoj, M.R.P. Kurup, Synthesis and EPR spectral studies of manganese(II) complexes derived from pyridine-2-carbaldehyde based N(4)-substituted thiosemicarbazones: Crystal structure of one complex, Polyhedron 26 (2007) 5088–5094.
[37] A.W. Addison, T.N. Rao, J. Reedijk, J. Van Rijn, G.C. Verschoor, Synthesis, structure, and spectroscopic properties of copper(II) compounds containing nitrogen–sulphur donor ligands; the crystal and molecular structure of aqua[1,7-bis(N-methylbenzimidazol-2′-yl)-2,6-dithiaheptane]copper(II) perchlorate, J. Chem. Soc., Dalton Trans. (1984) 1349.
[38] T.A. Reena, M.R.P. Kurup, Copper(II) complexes derived from di-2-pyridyl ketone-N4-phenyl-3-semicarbazone: Synthesis and spectral studies, Spectrochim. Acta A 76 (2010) 322–327.
[39] S.R. Sheeja, N.A. Mangalam, M. Sithambaresan, M.R.P. Kurup, G. Serdaroğlu, S. Kaya, Spectral studies and quantum chemical ab initio calculations for Copper(II) complexes of two heterocyclic aroylhydrazones, J. Mol. Struct. 1245 (2021) 131001.
[40] R.J. Kunnath, M. Sithambaresan, A.A. Aravindakshan, A. Natarajan, M.R.P. Kurup, The ligating versatility of pseudohalides like thiocyanate and cyanate in copper(II) complexes of 2-benzoylpyridine semicarbazone, Polyhedron 113 (2016) 73–80.
[41] V.L. Siji, M.R. Sudarsanakumar, S. Suma, M.R.P. Kurup, Synthesis, characterization and physiochemical information, along with antimicrobial studies of some metal complexes derived from an ON donor semicarbazone ligand, Spectrochim. Acta A76 (2010) 22–28.
[42] K. Jayakumar, M. Sithambaresan, N. Aiswarya, M.R.P. Kurup, Synthesis and spectral characterization of mono- and binuclear copper(II) complexes derived from 2-benzoylpyridine-N4-methyl-3-thiosemicarbazone: Crystal structure of a novel sulfur bridged copper(II) box-dimer, Spectrochim. Acta A139 (2015) 28–36.
[43] N.A. Mangalam, M.R.P. Kurup, Versatile binding properties of a di-2-pyridyl ketone nicotinoylhydrazone ligand: Crystal structure of a Cu(II) complex, Spectrochim. Acta A 78 (2011) 926–934.
[44] S.R. Layana, S.R Saritha, L. Anitha, M. Sithambaresan, M.R. Sudarsanakumar, S. Suma, Synthesis, spectral characterization and structural studies of a novel O, N, O donor semicarbazone and its binuclear copper complex with hydrogen bond stabilized lattice, J. Mol. Struct. 1157 (2018) 579–586.
[45] M. Joseph, V. Suni, M.R.P. Kurup, M. Nethaji, A. Kishore, S.G. Bhat, Structural, spectral and antimicrobial activities of copper(II) complexes of 2-benzoylpyridine N(4)–cyclohexyl thiosemicarbazones, Polyhedron 23 (2004) 3069–3080.
[46] P.R.S. Chandran, U.S.S. Mol, R. Drisya, M.R. Sudarsanakumar, M.R.P. Kurup, Structural studies of poly [(μ_2-acetato)(μ_3-5-aminoisophthalato) diaquacerium(III) monohydrate]: A new three dimensional fluorescent metal-organic framework constructed from dimers of CeO_9 polyhedra with hydrophilic 'S'shaped channels, J. Mol. Struct. 1137 (2017) 396–402, doi:10.1016/j.molstruc.2017.02.024.
[47] K. Jayakumar, M. Sithambaresan, A.A. Aravindakshan, M.R.P. Kurup, Synthesis and spectral characterization of copper(II) complexes derived from 2-benzoylpyridine-N4, N4-dimethyl-3-thiosemicarbazone: Crystal structure of a binuclear complex, Polyhedron 75 (2014) 50.
[48] F. Sevgi, U. Bagkesici, A.N. Kursunlu, E. Guler, Fe(III), Co(II), Ni(II), Cu(II) and Zn(II) complexes of Schiff bases based-on glycine and phenylalanine: synthesis, magnetic/thermal properties and antimicrobial activity, J. Mol. Struct. 1154 (2018) 256–260.
[49] A.K. Patel, R.N. Jadeja, H. Roy, R.N. Patel, S.K. Patel, R.J. Butcher, M. Cortijo, S. Herrero, Copper(II) hydrazone complexes with different nuclearities and geometries: Synthesis, structural characterization, antioxidant SOD activity and antiproliferative properties, Polyhedron 186 (2020) 114624.
[50] L. Latheef, M.R.P. Kurup, Spectral and structural studies of copper(II) complexes of thiosemicarbazones derived from salicylaldehyde and containing ring incorporated at N(4)-position, Spectrochim. Acta A 70 (2008) 86–93.
[51] M.R.P. Kurup, B. Varghese, M. Sithambaresan, S. Krishnan, S.R. Sheeja, Synthesis, spectral characterization and crystal structure of copper(II) complexes of 2-benzoylpyridine-N(4)-phenylsemicarbazone, Polyhedron 30 (2011) 70.
[52] L. Tom, N. Aiswarya, S.S. Sreejith, M.R.P. Kurup, Self-organized three dimensional architectures based on non-covalent interactions in square planar Cu(II) thiosemicarbazone: Solvent mediated crystallization and EPR based correlation study, Inorg. Chim. Acta 473 (2018) 223–235.
[53] E.B. Seena, M.R.P. Kurup, Spectral and structural studies of mono- and binuclear copper(II) complexes of salicylaldehyde N(4)-substituted thiosemicarbazones, Polyhedron 26 (2007) 829–836.
[54] E.B. Seena, M. Sithambaresan, S. Vasudevan, M.R.P. Kurup, Structural and spectral characterization of Cu(II) complexes of N(4)-substituted thiosemicarbazones derived from 2-hydroxyacetophenone: Crystal structure of a dinuclear Cu(II) complex, J. Chem. Sci. 132 (2020) 1–11.
[55] N. Uludag, G. Serdaroglu, ChemistrySelect 4 (2019) 6870-6878.
[56] G. Serdaroglu, Res. Chem. Intermediate. 46 (2020) 961–982.
[57] G. Serdaroglu, N. Uludag, Vib. Spectrosc. 111 (2020) 103156.
[58] G. Serdaroglu, N. Uludag, J. Struct. Chem. 60 (8) (2019) 1267–1284.
[59] G. Serdaroglu, Int. J. Quantum Chem. 111 (2011) 3938–3948.
[60] G. Serdaroglu, J.V. Ortiz, Struct. Chem. 28 (2017) 957–964.
[61] H. Kumar, T. Dhanda, J. Mol. Liq. 327 (2021) 114847.
[62] a) J.M. Jacob, M.R.P. Kurup, K. Nisha, G. Serdaroglu, S. Kaya, Polyhedron 189 (2020) 114736; b) P.K. Maniyampara, L.K. Suresh, K. Jayakumar, E. Manoj, M.R.P. Kurup, J. Mol. Struct. 1275 (2023) 134680.
[63] G. Serdaroglu, N. Sahin, M.N.Tahir Ustün, C. Arıcı, N. Gürbüz, I. Ozdemir, Polyhedron 204 (2021) 115281.
[64] K. Jayakumar, E.B. Seena, M.R.P. Kurup, S. Kaya, G. Serdaroğlu, E. Suresh, R. Marzouki, J. Mol. Struct. 1253 (2022) 132257.
[65] R.G. Parr, J.L. Gázquez, J. Phys. Chem. 97 (1993) 3939–3940.
[66] R.G. Parr, P.K. Chattaraj, Principle of maximum hardness, J. Am. Chem. Soc. 113 (1991) 1854–1855.
[67] S. Kaya, P.K. Chattaraj, G. Serdaroğlu, Polyhedron 202 (2021) 115207.